Annular Component Transient Thermoelastic Analysis Using a State Space Approach

Woon Yik Yong

Patrick S. Keogh
e-mail: enspsk@bath.ac.uk

Department of Mechanical Engineering,
University of Bath,
Bath BA2 7AY,
United Kingdom

Annular components are used widely in engineering systems and include bearing bushes and races, which may be exposed to extreme operating conditions. A method to establish the localized transient thermoelastic deformation of a homogeneous two-dimensional annular component is developed. The analysis is based on solving the thermoelasticity equations using a state space formulation for the Fourier components of the radial and tangential displacements. Two boundary conditions are considered, namely, rigid and resiliently mounted outer boundaries, both associated with stress free inner boundary conditions. The thermoelastic solution is then demonstrated for a transient temperature distribution induced by inner boundary frictional heating due to rotor contact, which is derived from a dynamic Hertzian pressure distribution. The application is to a relatively short auxiliary bearing for which a state of plane stress is appropriate. However, the thermoelastic analysis is generalized to cover cases of plane strain and plane stress.
[DOI: 10.1115/1.2768082]

Keywords: annular component, bearing, Fourier harmonics, state space, thermoelasticity

1 Introduction

There are many types of engineered annular components that are subjected to dynamic contact loads and frictional heating under operational conditions. A specific example given by Cole et al. [1] considers the influence of rotor contact on the internal dynamics and the bulk heat dissipation in a rolling element auxiliary bearing. The most common reason for failure of an auxiliary bearing in a magnetic bearing system is probably due to a combination of direct mechanical and thermoelastic stresses induced by rapidly varying localized friction forces in association with high surface slip velocities. Since the frictional heat input is transient, a general method for assessing thermoelastic distortion would be of benefit.

Johnson [2] gives a comprehensive overview of a range of contact problems. A more relevant guide for the contact problems associated with a rolling element bearing system is presented by Harris [3]. Most contact analyses are based on an elastic half space solution, i.e., for a small contact dimension compared to the radius of curvature. If the physical geometry and boundary conditions could be fully accounted for, the analysis would be able to cover local and global deformation cases of a real component. Chao and Tan [4] solve the annular thermoelastic problem subjected to a steady state point heat source using complex variable potentials. The heat source is applied within an annular region, where outer and inner boundaries are assumed to be isothermal.

The steady state thermoelastic problem for a half space subjected to a unit strength point temperature source was studied by Sternberg and McDowell [5] using Green's theorem. A classic half space study using transient thermoelastic Green's functions was published by Barber and Martin-Moran [6]. They utilized the Flamant point force solution together with the hoop stress induced by a unit impulse line heat source to obtain an equal and opposite surface pressure from the convolution theorem. The pressure was then superimposed with the original stress field to give a stress free surface condition. Difficulties were encountered in determining the stress field within the elastic half space due to the constraint imposed by the Flamant solution in calculating the offset pressure. Therefore, only displacements for particular distributions of transient surface heating were presented. Barber's later work with Azarkhin [7] overcame these issues by using the complex variable method. Other literature on frictional heating thermoelastic analysis including two-dimensional sliding contact is given by Yevtushenko and Kovalenko [8] and Yevtushenko and Kulchytsky-Zhyhailo [9]. A three-dimensional transient half space thermoelastic transient analysis is covered by Liu and Wang [10]. Most of these results are based on the knowledge of the associated heat conduction solutions that are presented by Carslaw and Jaeger [11].

Recently, Tarn and Wang [12] investigated the problem of laminated composite tubes subjected to various mechanical loading by means of a state space approach. The following work [13] used a similar approach to analyze the thermoelastic behavior of a cylindrical anisotropy model using a state space formalism. Papers by Ezzat et al. [14] and El-Maghraby and Yossef [15] also use state space approaches to investigate thermoelastic problems.

Analytical thermoelastic solutions arising from transient thermal conditions within an annular component have not been reported in the open literature. Since the thermal conditions are taken to be transient, the solution is not possible using a complex temperature potential. A state space formulation is therefore proposed in this paper since different mechanical boundary conditions may be incorporated without changing the overall form of the solution. Two boundary conditions are considered, namely, rigid and resiliently mounted outer boundaries, both with a stress free inner boundary condition.

2 Basic Thermoelastic Equations

Suppose that a homogeneous elastic body experiences change in temperature such that corresponding deformations may be considered to be quasistatic, i.e., elastic wave excitation is negligible. By ignoring body forces, the equilibrium equations are given in terms of polar coordinates (r, θ) as follows [16]:

Contributed by the Tribology Division of ASME for publication in the JOURNAL OF TRIBOLOGY. Manuscript received September 21, 2006; final manuscript received March 15, 2007. Review conducted by Michael Lovell.

$$\frac{\partial \sigma_r}{\partial r}+\frac{1}{r}\frac{\partial \tau_{r\theta}}{\partial \theta}+\frac{\sigma_r-\sigma_\theta}{r}=0$$

$$\frac{1}{r}\frac{\partial \sigma_\theta}{\partial \theta}+\frac{\partial \tau_{r\theta}}{\partial r}+\frac{2\tau_{r\theta}}{r}=0 \tag{1}$$

where σ_r and σ_θ are radial and hoop stresses, respectively, and $\tau_{r\theta}$ is the shear stress. In terms of radial (u_r) and tangential (v_θ) displacements, the strain-displacement equations are

$$\varepsilon_r=\frac{\partial u_r}{\partial r}$$

$$\varepsilon_\theta=\frac{u_r}{r}+\frac{1}{r}\frac{\partial v_\theta}{\partial \theta} \tag{2}$$

$$\gamma_{r\theta}=\frac{1}{r}\frac{\partial u_r}{\partial \theta}+\frac{\partial v_\theta}{\partial r}-\frac{v_\theta}{r}$$

where ε_r and ε_θ are principal radial and hoop strains, respectively, and $\gamma_{r\theta}$ is the shear strain. Under a temperature loading T, the two-dimensional stress-strain equations are

$$\sigma_r=\lambda[\beta\varepsilon_r+\nu\varepsilon_\theta-(1+\nu)\alpha_e T]$$

$$\sigma_\theta=\lambda[\beta\varepsilon_\theta+\nu\varepsilon_r-(1+\nu)\alpha_e T] \tag{3}$$

$$\tau_{r\theta}=G\gamma_{r\theta}$$

where G is the shear modulus, ν is Poisson's ratio, and α_e is the coefficient of thermal expansion. Equations (1) and (2) are applicable to any two-dimensional problem, while Eqs. (3) determine whether a state of plane strain or plane stress applies. The coefficients (λ,β) in Eqs. (3) should be distinguished as follows:

$$\lambda=\frac{2G}{1-2\nu}\quad \beta=1-\nu\quad \text{(plane strain case)} \tag{4}$$

$$\lambda=\frac{2G}{1-\nu}\quad \beta=1\quad \text{(plane stress case)} \tag{5}$$

Under this generalization, using Eqs. (1)–(3), the equilibrium equations may be expressed in terms of the elastic displacements according to

$$\frac{\partial^2 u_r}{\partial r^2}+\frac{1}{r}\frac{\partial u_r}{\partial r}-\frac{u_r}{r^2}+\frac{G}{\lambda\beta r^2}\frac{\partial^2 u_r}{\partial \theta^2}+\frac{(\nu\lambda+G)}{\lambda\beta r}\frac{\partial^2 v_\theta}{\partial r\partial\theta}-\frac{(\beta\lambda+G)}{\lambda\beta r^2}\frac{\partial v_\theta}{\partial\theta}=\frac{(1+\nu)}{\beta}\alpha_e\frac{\partial T}{\partial r}$$

$$\frac{\partial^2 v_\theta}{\partial r^2}+\frac{1}{r}\frac{\partial v_\theta}{\partial r}-\frac{v_\theta}{r^2}+\frac{\lambda\beta}{Gr^2}\frac{\partial^2 v_\theta}{\partial\theta^2}+\frac{(\nu\lambda+G)}{Gr}\frac{\partial^2 u_r}{\partial r\partial\theta}+\frac{(\beta\lambda+G)}{Gr^2}\frac{\partial u_r}{\partial\theta}=\frac{\lambda(1+\nu)}{Gr}\alpha_e\frac{\partial T}{\partial\theta} \tag{6}$$

For the practical bearing problem envisaged in this paper, a state of plane stress would be typical. However, the generality of Eqs. (6) is retained since the only detail is in the choice between Eqs. (4) and (5).

3 State Space Modeling

This technique is widely use in dynamic system modeling [17] but has received little attention for elasticity problems. A state space model consists of a state equation and an output equation. The state equation is a system of first order ordinary differential equations that describes fully the physical system behavior. The output equation represents user defined parameters of interest. The following analysis shows how the approach may be used to represent the distortional behavior of a thermally loaded annular component. The temperature T is generally time dependent; however, the quasistatic equations of elasticity are taken.

3.1 State Equation. The displacements are combined in the vector $\mathbf{w}=[u_r,v_\theta]^T$. Equations (6) may then be consolidated into the vector form

$$\frac{\partial^2\mathbf{w}}{\partial r^2}+\frac{1}{r}\frac{\partial\mathbf{w}}{\partial r}-\frac{\mathbf{w}}{r^2}+\frac{1}{r^2}\mathbf{M}_1\frac{\partial^2\mathbf{w}}{\partial\theta^2}+\frac{1}{r}\mathbf{M}_2\frac{\partial^2\mathbf{w}}{\partial r\partial\theta}+\frac{1}{r^2}\mathbf{M}_3\frac{\partial\mathbf{w}}{\partial\theta}=\frac{1}{r^2}\mathbf{f} \tag{7}$$

where

$$\mathbf{M}_1=\begin{bmatrix}G/\lambda\beta & 0\\ 0 & \lambda\beta/G\end{bmatrix}\quad \mathbf{M}_2=(\nu\lambda+G)\begin{bmatrix}0 & 1/\lambda\beta\\ 1/G & 0\end{bmatrix}$$

$$\mathbf{M}_3=(\lambda\beta+G)\begin{bmatrix}0 & -1/\lambda\beta\\ 1/G & 0\end{bmatrix}$$

and

$$\mathbf{f}=(1+\nu)\alpha_e r^2\left[\frac{1}{\beta}\frac{\partial T}{\partial r},\ \frac{\lambda}{Gr}\frac{\partial T}{\partial\theta}\right]^T$$

Now express the angular variation through Fourier series representations of $\mathbf{w}$ and T:

$$\mathbf{w}=\sum_{n=-\infty}^{\infty}\mathbf{w}_n e^{in\theta}\quad T=\sum_{n=-\infty}^{\infty}T_n e^{in\theta} \tag{8}$$

Equation (7) then yields

$$r^2\frac{\partial^2\mathbf{w}_n}{\partial r^2}+r\mathbf{B}_n\frac{\partial\mathbf{w}_n}{\partial r}-\mathbf{C}_n\mathbf{w}_n=\mathbf{f}_n \tag{9}$$

where the matrix coefficients are defined by

$$\mathbf{B}_n=\mathbf{I}+in\mathbf{M}_2\quad \mathbf{C}_n=\mathbf{I}+n^2\mathbf{M}_1-in\mathbf{M}_3 \tag{10}$$

and the right hand side input vector is

$$\mathbf{f}_n(r,t)=(1+\nu)\alpha_e r^2\left[\frac{1}{\beta}\frac{\partial T_n}{\partial r},\ i\frac{\lambda n}{Gr}T_n\right]^T \tag{11}$$

Equation (9) is a second order ordinary differential equation with variable coefficients. It can be transformed into an equation with constant coefficients by setting $r=e^z$:

$$\mathbf{W}_n(z,t)=\mathbf{w}_n(e^z,t) \tag{12}$$

which yields

$$\frac{\partial^2\mathbf{W}_n}{\partial z^2}+(\mathbf{B}_n-\mathbf{I})\frac{\partial\mathbf{W}_n}{\partial z}-\mathbf{C}_n\mathbf{W}_n=\mathbf{F}_n \tag{13}$$

where

$$\mathbf{F}_n(z,t)=(1+\nu)\alpha_e e^z\left[\frac{1}{\beta}\frac{\partial\hat{T}_n(z,t)}{\partial z},\ i\frac{\lambda n}{G}\hat{T}_n(z,t)\right]^T \tag{14}$$

and

$$\hat{T}_n(z,t)=T_n(e^z,t) \tag{15}$$

Although quasistatic elasticity equations are used, the time variable t is shown for completeness. Equation (13) may now be reduced to first order form through

$$\mathbf{X}_n=\frac{\partial\mathbf{W}_n}{\partial z}=\mathbf{W}_n'$$

$$\mathbf{X}_n'+(\mathbf{B}_n-\mathbf{I})\mathbf{X}_n-\mathbf{C}_n\mathbf{W}_n=\mathbf{F}_n \tag{16}$$

where $'$ denotes partial differentiation with respect to z. By defining the system state vector as

$$\mathbf{Z}_n(z,t) = \begin{bmatrix} \mathbf{W}_n(z,t) \\ \mathbf{X}_n(z,t) \end{bmatrix} \tag{17}$$

it follows that the state equation is

$$\mathbf{Z}_n'(z,t) = \mathbf{A}_n \mathbf{Z}_n(z,t) + \mathbf{E}_n(z,t) \tag{18}$$

where the constant coefficient system matrix is

$$\mathbf{A}_n = \begin{bmatrix} \mathbf{0} & \mathbf{I} \\ \mathbf{C}_n & \mathbf{I} - \mathbf{B}_n \end{bmatrix} \tag{19}$$

and the input vector is

$$\mathbf{E}_n(z,t) = \begin{bmatrix} \mathbf{0} \\ \mathbf{F}_n(z,t) \end{bmatrix} \tag{20}$$

3.2 General Solution of the State Equation. Equation (18) may be solved using an integrating factor to yield

$$\mathbf{Z}_n(z,t) = e^{\mathbf{A}_n(z-z_i)}\mathbf{Z}_n(z_i,t) + \int_{z_i}^{z} e^{\mathbf{A}_n(z-p)}\mathbf{E}_n(p,t)dp \tag{21}$$

The "initial" value $\mathbf{Z}_n(z_i,t)$ has yet to be determined. It must be related to mechanical boundary conditions. To make further progress, an output equation is defined.

3.3 Output Equation. The output equation defines the parameters that are of interest in terms of the state and input vectors:

$$\mathbf{Y}_n(z,t) = \mathbf{G}_n(z)\mathbf{Z}_n(z,t) + \mathbf{H}_n(z)\mathbf{E}_n(z,t) \tag{22}$$

For polar coordinates associated with the annular problem, it is appropriate to define

$$\mathbf{y}(r,\theta,t) = \sum_{n=-\infty}^{\infty} \mathbf{y}_n(r,t)e^{in\theta} \tag{23}$$

where $\mathbf{y}=[u_r, v_\theta, \sigma_r, \sigma_\theta, \tau_{r\theta}]^T$. Setting $r=e^z$ implies that

$$\mathbf{y}_n(r,t) = \mathbf{Y}_n(z,t) = [U_{rn}(z,t), V_{\theta n}(z,t), \Lambda_{rn}(z,t), \Lambda_{\theta n}(z,t), \Lambda_{r\theta n}(z,t)]^T \tag{24}$$

where

$$\begin{aligned} U_{rn}(z,t) &= u_{rn}(e^z,t) \\ V_{\theta n}(z,t) &= v_{\theta n}(e^z,t) \end{aligned} \tag{25}$$

and the radial derivatives implicit in Eqs. (3) imply that

$$\begin{aligned} \Lambda_{rn}(z,t) &= \lambda e^{-z}[\beta U_{rn}'(z,t) + \nu U_{rn}(z,t) + in\nu V_{\theta n}(z,t)] \\ &\quad - \lambda(1+\nu)\alpha_e \hat{T}_n(z,t) \\ \Lambda_{\theta n}(z,t) &= \lambda e^{-z}[\nu U_{rn}'(z,t) + \beta U_{rn}(z,t) + in\beta V_{\theta n}(z,t)] \\ &\quad - \lambda(1+\nu)\alpha_e \hat{T}_n(z,t) \\ \Lambda_{r\theta n}(z,t) &= Ge^{-z}[V_{\theta n}'(z,t) + inU_{rn}(z,t) - V_{\theta n}(z,t)] \end{aligned} \tag{26}$$

It is now possible to deduce that the matrices in the output equation (Eq. (22)) must have the forms

$$\mathbf{G}_n(z) = \begin{bmatrix} 1 & 0 & 0 & 0 \\ 0 & 1 & 0 & 0 \\ \lambda\nu e^{-z} & in\lambda\nu e^{-z} & \lambda\beta e^{-z} & 0 \\ \lambda\beta e^{-z} & in\lambda\beta e^{-z} & \lambda\nu e^{-z} & 0 \\ inGe^{-z} & -Ge^{-z} & 0 & Ge^{-z} \end{bmatrix}$$

$$\mathbf{H}_n(z) = \frac{iGe^{-z}}{n}\begin{bmatrix} 0 & 0 & 0 & 0 \\ 0 & 0 & 0 & 0 \\ 0 & 0 & 0 & 1 \\ 0 & 0 & 0 & 1 \\ 0 & 0 & 0 & 0 \end{bmatrix} \tag{27}$$

4 State Space Model With Physical Boundary Conditions

The state space representation of Eqs. (18) and (22) for the thermoelastic annular problem must be solved with appropriate mechanical boundary conditions. Two distinct boundary condition combinations are considered, namely,

- (B1) rigid outer boundary ($r=r_o$) with stress free inner boundary ($r=r_i$)
- (B2) resiliently mounted outer boundary ($r=r_o$) with stress free inner boundary ($r=r_i$)

At this stage, the analysis is applicable to any dynamic two-dimensional temperature distribution $T(r,\theta,t)$. Thermal boundary and initial conditions will of course determine the temperature, but they do not need to be specified at this point. The following subsections demonstrate the procedure for determining the unknown state vector $\mathbf{Z}_n(z_i,t)$, which is associated with the inner boundary.

4.1 Rigid Outer Boundary (B1). Consider the two-dimensional annulus with a fixed outer boundary, as shown in Fig. 1(*a*). The inner and outer radii are r_i and r_o, respectively, and after transformation, $z_i=\ln r_i$ and $z_o=\ln r_o$. If the inner boundary is stress free, the boundary conditions are

$$\begin{aligned} \sigma_r(r_i,t) &= \tau_{r\theta}(r_i,t) = 0 \\ u_r(r_o,t) &= v_\theta(r_o,t) = 0 \end{aligned} \tag{28}$$

To determine $\mathbf{Z}_n(z_i,t)=\mathbf{c}_n^{\text{rig}}(t)$, the state vector at the outer boundary is expressed from Eq. (21) as

$$\mathbf{Z}_n(z_o,t) = e^{\mathbf{A}_n(z_o-z_i)}\mathbf{c}_n^{\text{rig}}(t) + \int_{z_i}^{z_o} e^{\mathbf{A}_n(z_o-p)}\mathbf{E}_n(p,t)dp \tag{29}$$

The inner and outer boundary conditions in Eq. (28) imply that the output vector may be expressed at $z=z_i,z_o$ according to

$$\begin{aligned} \mathbf{Y}_n(z_i,t) &= [U_{rn}(z_i,t), V_{\theta n}(z_i,t), 0, \Lambda_{\theta n}(z_i,t), 0]^T = \mathbf{G}_n(z_i)\mathbf{c}_n^{\text{rig}}(t) \\ &\quad + \mathbf{H}_n(z_i)\mathbf{E}_n(z_i,t) \\ \mathbf{Y}_n(z_o,t) &= [0, 0, \Lambda_{rn}(z_o,t), \Lambda_{\theta n}(z_o,t), \Lambda_{r\theta n}(z_o,t)]^T = \mathbf{G}_n(z_o)\mathbf{Z}_n(z_o,t) \\ &\quad + \mathbf{H}_n(z_o)\mathbf{E}_n(z_o,t) \end{aligned} \tag{30}$$

The hoop stress components are not specifically required to satisfy the boundary conditions. Therefore, by deleting the fourth rows in Eqs. (30), the following 2×2 subblock forms may be derived:

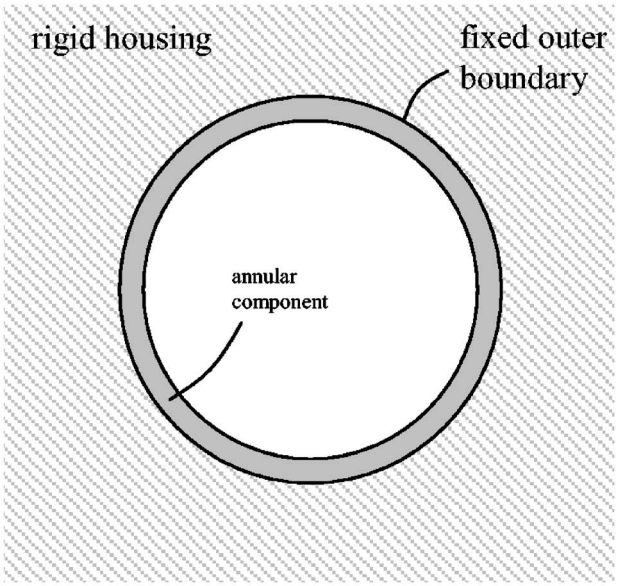

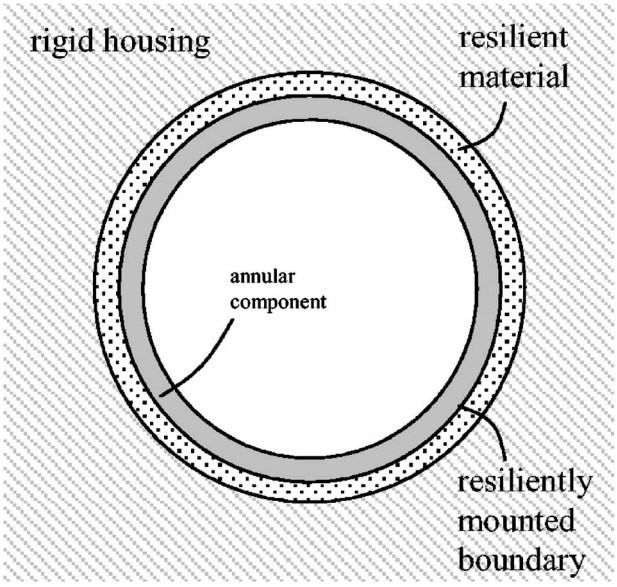

Fig. 1 Mounting configurations for annular component: (*a*) rigid outer boundary and (*b*) resiliently mounted outer boundary

$$\begin{bmatrix} \mathbf{U}_n(z_i,t) \\ \mathbf{0} \end{bmatrix} = \begin{bmatrix} \mathbf{I} & \mathbf{0} \\ \mathbf{G}_{n21}(z_i) & \mathbf{G}_{n22}(z_i) \end{bmatrix} \begin{bmatrix} \mathbf{c}_{n1}^{\text{rig}}(t) \\ \mathbf{c}_{n2}^{\text{rig}}(t) \end{bmatrix} + \begin{bmatrix} \mathbf{0} & \mathbf{0} \\ \mathbf{0} & \mathbf{H}_{n22}(z_i) \end{bmatrix} \times \begin{bmatrix} \mathbf{0} \\ \mathbf{F}_n(z_i,t) \end{bmatrix} \tag{31}$$

and

$$\begin{bmatrix} \mathbf{0} \\ \mathbf{\Lambda}_n(z_o,t) \end{bmatrix} = \begin{bmatrix} \mathbf{I} & \mathbf{0} \\ \mathbf{G}_{n21}(z_o) & \mathbf{G}_{n22}(z_o) \end{bmatrix} \begin{bmatrix} \mathbf{\Delta}_{n11} & \mathbf{\Delta}_{n12} \\ \mathbf{\Delta}_{n21} & \mathbf{\Delta}_{n22} \end{bmatrix} \begin{bmatrix} \mathbf{c}_{n1}^{\text{rig}}(t) \\ \mathbf{c}_{n2}^{\text{rig}}(t) \end{bmatrix} + \begin{bmatrix} \mathbf{I} & \mathbf{0} \\ \mathbf{G}_{n21}(z_o) & \mathbf{G}_{n22}(z_o) \end{bmatrix} \begin{bmatrix} \mathbf{\Phi}_{n1}(t) \\ \mathbf{\Phi}_{n2}(t) \end{bmatrix} + \begin{bmatrix} \mathbf{0} & \mathbf{0} \\ \mathbf{0} & \mathbf{H}_{n22}(z_o) \end{bmatrix} \times \begin{bmatrix} \mathbf{0} \\ \mathbf{F}_n(z_o,t) \end{bmatrix} \tag{32}$$

Here,

$$\mathbf{U}_n(z,t) = \begin{bmatrix} U_{rn}(z,t) \\ V_{\theta n}(z,t) \end{bmatrix} \quad \mathbf{\Lambda}_n(z,t) = \begin{bmatrix} \Lambda_{rn}(z,t) \\ \Lambda_{r\theta n}(z,t) \end{bmatrix} \quad \mathbf{c}_n^{\text{rig}}(t) = \begin{bmatrix} \mathbf{c}_{n1}^{\text{rig}}(t) \\ \mathbf{c}_{n2}^{\text{rig}}(t) \end{bmatrix}$$

$$\mathbf{G}_{n21}(z) = e^{-z} \begin{bmatrix} \lambda\nu & in\lambda\nu \\ inG & -G \end{bmatrix} \quad \mathbf{G}_{n22}(z) = e^{-z} \begin{bmatrix} \lambda\beta & 0 \\ 0 & G \end{bmatrix}$$

$$\mathbf{H}_{n22}(z) = \frac{iGe^{-z}}{n} \begin{bmatrix} 0 & 1 \\ 0 & 0 \end{bmatrix}$$

$$\begin{bmatrix} \mathbf{\Delta}_{n11} & \mathbf{\Delta}_{n12} \\ \mathbf{\Delta}_{n21} & \mathbf{\Delta}_{n22} \end{bmatrix} = e^{\mathbf{A}_n(z_o - z_i)} \quad \begin{bmatrix} \mathbf{\Phi}_{n1}(t) \\ \mathbf{\Phi}_{n2}(t) \end{bmatrix} = \int_{z_i}^{z_o} e^{\mathbf{A}_n(z_o - p)} \mathbf{E}_n(p,t)\,dp$$

Setting

$$\begin{bmatrix} \mathbf{J}_{n11} & \mathbf{J}_{n12} \\ \mathbf{J}_{n21} & \mathbf{J}_{n22} \end{bmatrix} = \begin{bmatrix} \mathbf{I} & \mathbf{0} \\ \mathbf{G}_{n21}(z_o) & \mathbf{G}_{n22}(z_o) \end{bmatrix} \begin{bmatrix} \mathbf{\Delta}_{n11} & \mathbf{\Delta}_{n12} \\ \mathbf{\Delta}_{n21} & \mathbf{\Delta}_{n22} \end{bmatrix} \tag{33}$$

the second block row of Eq. (31) and the first block row of Eq. (32) yield

$$\begin{gathered} \mathbf{G}_{n21}(z_i)\mathbf{c}_{n1}^{\text{rig}}(t) + \mathbf{G}_{n22}(z_i)\mathbf{c}_{n2}^{\text{rig}}(t) + \mathbf{H}_{n22}(z_i)\mathbf{F}_n(z_i,t) = \mathbf{0} \\ \mathbf{J}_{n11}\mathbf{c}_{n1}^{\text{rig}}(t) + \mathbf{J}_{n12}\mathbf{c}_{n2}^{\text{rig}}(t) + \mathbf{\Phi}_{n1}(t) = \mathbf{0} \end{gathered} \tag{34}$$

Therefore, the required vector is

$$\mathbf{c}_n^{\text{rig}}(t) = -\begin{bmatrix} \mathbf{G}_{n21}(z_i) & \mathbf{G}_{n22}(z_i) \\ \mathbf{J}_{n11} & \mathbf{J}_{n12} \end{bmatrix}^{-1} \begin{bmatrix} \mathbf{H}_{n22}(z_i)\mathbf{F}_n(z_i,t) \\ \mathbf{\Phi}_{n1}(t) \end{bmatrix} \tag{35}$$

4.2 Resiliently Mounted Outer Boundary (B2). Consider now a resiliently mounted annulus, where outer boundary movement is permissible (Fig. 1(*b*)). The annulus is subjected to thermal loading, and deformation at the outer boundary is equilibrated by resilient constraints. If the constraints are considered to be linear mechanical elements, the outer boundary conditions may be expressed as

$$\begin{gathered} \sigma_r(r_o,t) + k_r u_r(r_o,t) = 0 \\ \sigma_\theta(r_o,t) + k_\theta v_\theta(r_o,t) = 0 \end{gathered} \tag{36}$$

where k_r and k_θ are stiffnesses per unit width opposing radial and tangential displacements, respectively. In Eqs. (36), the tangential constraint is considered to induce hoop stress in the outer boundary. In some applications, it may be more appropriate to replace the hoop stress by the shear stress. In either case, $\mathbf{Z}_n(z_i,t) = \mathbf{c}_n^{\text{res}}(t)$ must be established. The output vector at the outer boundary can be written as

$$\begin{aligned} \mathbf{Y}_n(z_o,t) &= [-k_r^{-1}\Lambda_{rn}(z_o,t), \\ &\quad -k_\theta^{-1}\Lambda_{\theta n}(z_o,t), \Lambda_{rn}(z_o,t), \Lambda_{\theta n}(z_o,t), \Lambda_{r\theta n}(z_o,t)]^T \\ &= \mathbf{G}_n(z_o)\mathbf{Z}_n(z_o,t) + \mathbf{H}_n(z_o)\mathbf{E}_n(z_o,t) \end{aligned} \tag{37}$$

where $\mathbf{Z}_n(z_o,t) = e^{\mathbf{A}_n(z_o - z_i)}\mathbf{c}_n^{\text{res}}(t) + \int_{z_i}^{z_o} e^{\mathbf{A}_n(z_o - p)}\mathbf{E}_n(p,t)\,dp$. Removing the shear stress term from the last row of the output vector in Eq. (37), the residual four-dimensional vector may be partitioned into a pair of two-dimensional vectors. This yields the reduced form to represent the boundary conditions of Eq. (36):

$$\begin{bmatrix} -\mathbf{K}^{-1}\tilde{\mathbf{\Lambda}}_n(z_o,t) \\ \tilde{\mathbf{\Lambda}}_n(z_o,t) \end{bmatrix} = \begin{bmatrix} \tilde{\mathbf{J}}_{n11} & \tilde{\mathbf{J}}_{n12} \\ \tilde{\mathbf{J}}_{n21} & \tilde{\mathbf{J}}_{n22} \end{bmatrix} \begin{bmatrix} \mathbf{c}_{n1}^{\text{res}}(t) \\ \mathbf{c}_{n2}^{\text{res}}(t) \end{bmatrix} + \begin{bmatrix} \mathbf{R}_{n1}(t) \\ \mathbf{R}_{n2}(t) \end{bmatrix} \tag{38}$$

where

$$\mathbf{K} = \begin{bmatrix} k_r & 0 \\ 0 & k_\theta \end{bmatrix} \quad \tilde{\mathbf{\Lambda}}_n(z,t) = \begin{bmatrix} \Lambda_{rn}(z,t) \\ \Lambda_{\theta n}(z,t) \end{bmatrix} \quad \mathbf{c}_n^{\text{res}}(t) = \begin{bmatrix} \mathbf{c}_{n1}^{\text{res}}(t) \\ \mathbf{c}_{n2}^{\text{res}}(t) \end{bmatrix}$$

$$\begin{bmatrix} \tilde{\mathbf{J}}_{n11} & \tilde{\mathbf{J}}_{n12} \\ \tilde{\mathbf{J}}_{n21} & \tilde{\mathbf{J}}_{n22} \end{bmatrix} = \begin{bmatrix} \mathbf{I} & \mathbf{0} \\ \tilde{\mathbf{G}}_{n21}(z_o) & \tilde{\mathbf{G}}_{n22}(z_o) \end{bmatrix} \begin{bmatrix} \boldsymbol{\Delta}_{n11} & \boldsymbol{\Delta}_{n12} \\ \boldsymbol{\Delta}_{n21} & \boldsymbol{\Delta}_{n22} \end{bmatrix}$$

$$\mathbf{R}_n(t) = \begin{bmatrix} \mathbf{I} & \mathbf{0} \\ \tilde{\mathbf{G}}_{n21}(z_o) & \tilde{\mathbf{G}}_{n22}(z_o) \end{bmatrix} \begin{bmatrix} \boldsymbol{\Phi}_{n1}(t) \\ \boldsymbol{\Phi}_{n2}(t) \end{bmatrix} + \tilde{\mathbf{H}}_{n22}(z_o)\mathbf{F}_n(z_o,t)$$

$$\tilde{\mathbf{G}}_{n21}(z) = e^{-z} \begin{bmatrix} \lambda\nu & in\lambda\nu \\ \lambda\beta & in\lambda\beta \end{bmatrix} \quad \tilde{\mathbf{G}}_{n22}(z) = e^{-z} \begin{bmatrix} \lambda\beta & 0 \\ \lambda\nu & 0 \end{bmatrix}$$

$$\tilde{\mathbf{H}}_{n22}(z) = \frac{iGe^{-z}}{n} \begin{bmatrix} 0 & 1 \\ 0 & 1 \end{bmatrix}$$

Manipulation of the subblock rows of Eq. (38) gives

$$(\mathbf{K}\tilde{\mathbf{J}}_{n11} + \tilde{\mathbf{J}}_{n21})\mathbf{c}_{n1}^{\text{res}}(t) + (\mathbf{K}\tilde{\mathbf{J}}_{n12} + \tilde{\mathbf{J}}_{n22})\mathbf{c}_{n2}^{\text{res}}(t) + \mathbf{K}\mathbf{R}_{n1}(t) + \mathbf{R}_{n2}(t) = \mathbf{0} \tag{39}$$

To determine $\mathbf{c}_n^{\text{res}}(t)$, a second relation, similar to Eq. (31) for the inner boundary, is

$$\begin{bmatrix} \mathbf{U}_n(z_i,t) \\ \mathbf{0} \end{bmatrix} = \begin{bmatrix} \mathbf{I} & \mathbf{0} \\ \tilde{\mathbf{G}}_{n21}(z_i) & \tilde{\mathbf{G}}_{n22}(z_i) \end{bmatrix} \begin{bmatrix} \mathbf{c}_{n1}^{\text{res}}(t) \\ \mathbf{c}_{n2}^{\text{res}}(t) \end{bmatrix} + \begin{bmatrix} \mathbf{0} & \mathbf{0} \\ \mathbf{0} & \tilde{\mathbf{H}}_{n22}(z_i) \end{bmatrix} \times \begin{bmatrix} \mathbf{0} \\ \mathbf{F}_n(z_i,t) \end{bmatrix} \tag{40}$$

Taking the second block row of Eq. (40) gives

$$\tilde{\mathbf{G}}_{n21}(z_i)\mathbf{c}_{n1}^{\text{res}}(t) + \tilde{\mathbf{G}}_{n22}(z_i)\mathbf{c}_{n2}^{\text{res}}(t) + \tilde{\mathbf{H}}_{n22}(z_i)\mathbf{F}_n(z_i,t) = \mathbf{0} \tag{41}$$

Equations (39) and (41) now yield

$$\mathbf{c}_n^{\text{res}}(t) = -\begin{bmatrix} \tilde{\mathbf{G}}_{n21}(z_i) & \tilde{\mathbf{G}}_{n22}(z_i) \\ \mathbf{K}\tilde{\mathbf{J}}_{n11} + \tilde{\mathbf{J}}_{n21} & \mathbf{K}\tilde{\mathbf{J}}_{n21} + \tilde{\mathbf{J}}_{n22} \end{bmatrix}^{-1} \begin{bmatrix} \tilde{\mathbf{H}}_{n22}(z_i)\mathbf{F}_n(z_i,t) \\ \mathbf{K}\mathbf{R}_{n1}(t) + \mathbf{R}_{n2}(t) \end{bmatrix} \tag{42}$$

5 Thermoelastic Line Source Green's Function

5.1 Transient Temperature Distribution. Consider the annular component to be subjected to inner boundary heating. The temperature distribution in the component can be evaluated using a convolution of a Green's function solution and the surface heat source distribution. The form of the Green's function solution for an instantaneous unit line source at $\theta=t=0$ under adiabatic boundary conditions may be stated in Fourier series form [11]

$$T_G(r,\theta,t) = \sum_{n=-\infty}^{\infty} T_{Gn}(r,t)e^{in\theta} \tag{43}$$

The harmonic coefficients in the θ coordinate are time dependent; hence, they may be expressed in terms of an inverse Laplace transform

$$T_{Gn}(r,t) = \frac{1}{2\pi i}\int_{c-i\infty}^{c+i\infty} \bar{T}_{Gn}(r,s)e^{st}ds \tag{44}$$

with

$$\bar{T}_{Gn}(r,s) = -\frac{K_n(\gamma r)I_n'(\gamma r_o) - I_n(\gamma r)K_n'(\gamma r_o)}{2\pi K_b \gamma r_i[K_n'(\gamma r_i)I_n'(\gamma r_o) - I_n'(\gamma r_i)K_n'(\gamma r_o)]}$$

where I_n and K_n are modified Bessel functions, $\gamma=\sqrt{s/\kappa_b}$, K_b is the thermal conductivity, and κ_b is the thermal diffusivity.

There are well known techniques that may be used to evaluate Eq. (44) numerically, including completion of the contour of integration in the left half of the complex plane. However, there are issues relating to poor series convergence with the use of Eq. (43) for localized heat input problems. An improved representation is derived in Ref. [18] by comparison with the local half space Green's function T_{GH}. The complete solution has the form

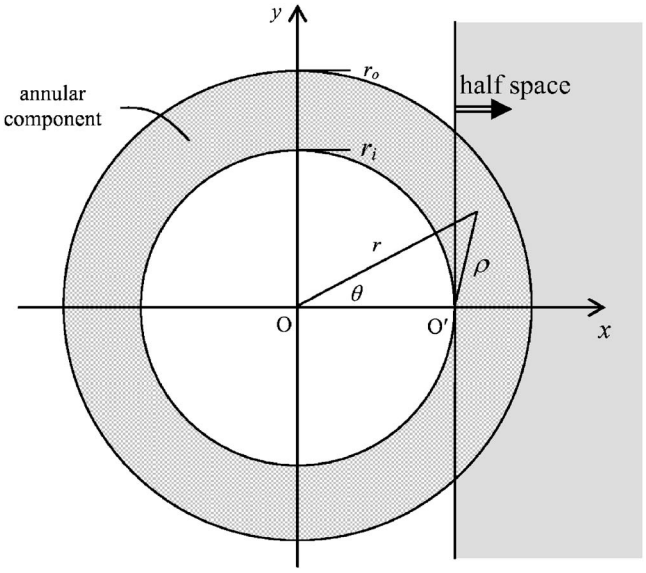

Fig. 2 Coordinate systems for superimposed annular and half space regions. The line source location is the axial line through *O′*.

$$T_G(r,\theta,t) = T_{GH}(r,\theta,t) - \frac{1}{2\pi K_b}\int_0^t g_b(\tau)T_{GH}(r,\theta,t-\tau)d\tau + \sum_{n=-\infty}^{\infty} T_{GRn}(r,t)e^{in\theta} \tag{45}$$

where

$$T_{GH}(r,\theta,t) = \frac{e^{-\rho^2/4\kappa_b t}}{2\pi K_b t}$$

$$g_b(t) = \frac{\sqrt{\kappa_b}}{2r_i}\left[\frac{1}{\sqrt{\pi t}} - \frac{\sqrt{\kappa_b}}{2r_i}e^{\kappa_b t/4r_i^2}\,\text{erfc}(\sqrt{\kappa_b t}/2r_i)\right]$$

with $\rho=\sqrt{r^2+r_i^2-2rr_i\cos\theta}$. The residual series in Eq. (45) is, in fact, convergent for all $t\geqslant 0$ and all θ.

5.2 Displacement and Stress Issues. The transient temperature harmonics from Eq. (43) may be used directly in the input vector of Eq. (11) to derive the displacements and stresses appropriate for either of the boundary conditions (B1) or (B2). Corresponding to T_G, let the thermoelastic displacement and stress vector of Eq. (23) be denoted in the form

$$\mathbf{y}_G(r,\theta,t) = \begin{bmatrix} \mathbf{w}_G(r,\theta,t) \\ \boldsymbol{\sigma}_G(r,\theta,t) \end{bmatrix} = \begin{bmatrix} \sum_{n=-\infty}^{\infty} \mathbf{w}_{Gn}(r,t)e^{in\theta} \\ \sum_{n=-\infty}^{\infty} \boldsymbol{\sigma}_{Gn}(r,t)e^{in\theta} \end{bmatrix} \tag{46}$$

where $\mathbf{w}_G=[u_{Gr}, v_{G\theta}]^T$ and $\boldsymbol{\sigma}_G=[\sigma_{Gr}, \sigma_{G\theta}, \tau_{Gr\theta}]^T$. The harmonics may be determined using the methodology described in Sec. 4. Since the singular nature of the thermal Green's function will affect displacements and stresses at $\theta=t=0$, the resulting Fourier series in Eq. (46) will also be poorly convergent at short time scales. Hence, it is appropriate to improve matters by introducing half space displacement solutions to represent the singular behavior in more detail, in particular, close to the line source. Figure 2 shows a half space that has been superimposed onto a cross sec-

Table 1 Data used for thermoelastic case study

Auxiliary bearing	Operating parameters
Inner radius $r_i=20.0$ mm	Radial stiffness/length $k_r=3.45\times10^{13}$ N/m^3
Outer radius $r_o=22.0$ mm	Tangential stiffness/length $k_\theta=5\times10^{11}$ N/m^3
Width $l_b=6.0$ mm	Contact angle $\theta_0=195$ rad
Density $\rho_b=7850$ kg/m^3	Heat flux/length $q_0=1.36\times10^9$ W/m^3
Specific heat $c_b=500$ J/kg K	Contact duration frequency $\omega_c=159$ rad/s
Conductivity $K_b=50$ W/m K	
Diffusivity $\kappa_b=1.27\times10^{-5}$ m^2/s	
Thermal expansion coefficient $\alpha_e=11\times10^{-6}$/K	
Shear modulus $G=80\times10^9$ N/m^2	
Poisson ratio $\nu=0.3$	

tion of the annular component. The half space surface and the component inner surface coincide along the axial line $r=r_i$, $\theta=0$ through the point O', which is also the location of the line source. Referring to the Cartesian coordinates shown in Fig. 2, Barber and Martin-Moran [6] derived half space surface displacements that satisfy stress free boundary conditions:

$$u_{GHx}(Y,t)=\frac{\alpha_e}{\pi\rho_b c_b\sqrt{\kappa_b t}}\frac{(1+\nu)}{(\beta+\nu)}F_1(Y)$$
$$u_{GHy}(Y,t)=\frac{\alpha_e}{\pi\rho_b c_b\sqrt{\kappa_b t}}\frac{(1+\nu)}{(\beta+\nu)}\left(\frac{1-e^{-Y^2}}{Y}\right) \tag{47}$$

where $Y=y/2\sqrt{\kappa_b t}$, ρ_b is the density, c_b is the specific heat, and

$$F_1(Y)=\frac{2}{\sqrt{\pi}}\frac{e^{-Y^2}}{Y}\int_0^Y e^{S^2}dS \tag{48}$$

Although the displacement forms of Eq. (47) are valid on the half space surface only, they are useful for the annular component problem. The surface displacements of Eq. (47) are "continued" away from the surface by replacing the surface coordinate Y with a radial coordinate $R=\rho/2\sqrt{\kappa_b t}$. The singular behavior in the continued radial and tangential displacements is then contained in the forms

$$\bar{u}_{GHr}(r,\theta,t)=u_{GHx}(R,t)\cos\theta=\sum_{n=-\infty}^{\infty}\bar{u}_{GHrn}(r,t)e^{in\theta}$$
$$\bar{v}_{GH\theta}(r,\theta,t)=\frac{r_i\tan\theta}{R}u_{GHy}(R,t)\cos\theta=\sum_{n=-\infty}^{\infty}\bar{v}_{GH\theta n}(r,t)e^{in\theta} \tag{49}$$

where terms involving $\sin\theta$ have not been included since they are bounded at $\theta=0$. The multiplying factor $(r_i\tan\theta/R)$ has been introduced for analytical convenience, as apparent in the Appendix, but it does not change the nature of the singular behavior. Expressions for the harmonic terms in Eq. (49) are provided in the Appendix. It is now evident that the displacement terms in Eq. (46) may be rewritten in the form

$$\mathbf{w}_G(r,\theta,t)=\bar{\mathbf{w}}_{GH}(r,\theta,t)+\sum_{n=-\infty}^{\infty}\mathbf{w}_{GRn}(r,t)e^{in\theta} \tag{50}$$

where $\bar{\mathbf{w}}_{GH}=[\bar{u}_{GH},\bar{v}_{GH\theta}]^T$ and $\mathbf{w}_{GRn}=\mathbf{w}_{Gn}-[\bar{u}_{GHrn},\bar{v}_{GH\theta n}]^T$. The benefits of using Eq. (50) will be demonstrated in Sec. 6. It is noted that the introduction of $\bar{\mathbf{w}}_{GH}$ does not change the solution so that the correct boundary conditions are still satisfied. The purpose of $\bar{\mathbf{w}}_{GH}$ is to increase the rate of convergence of the residual Fourier series in Eq. (50).

It remains to comment on whether the same technique may be applied to obtain a more efficient representation for the stresses in Eq. (46). Although the nominal forms of Eq. (49) are deduced from stress free half space surface displacements, they are not true elastic displacement solutions. Furthermore, when Y is replaced by $R=\rho/2\sqrt{\kappa_b t}$ in Eq. (47), the stress free half space surface condition is no longer satisfied according to Hooke's law. Therefore, the stress forms of Eq. (46) will be unchanged for the present paper.

6 Case Study Example

6.1 Validation of the Solution Method. The analysis of Sec. 4 was introduced to enable efficient evaluation of transient thermoelastic distortion. This was developed in Secs. 5.1 and 5.2 to define thermoelastic Green's functions that are useful for short time scales and localized problems. There is some complexity in the methodology, which raises the question of validation. At present, experimental results in the open literature for transient thermoelastic distortion are very limited. In fact, no meaningful comparison with the analysis could be made. It was therefore decided upon to compare analytical results with those predicted by already validated finite element software [19].

A key stage in the validation process is to ensure that for a given temperature distribution, the thermoelastic displacements are correctly predicted. The geometric and material data for the auxiliary bearing specified in Table 1 were selected. A transient temperature distribution was evaluated as part of the finite element solution by applying a constant heat flux on the inner surface of the bearing over an arclength of 0.155 rad. After 20 s, the temperature distribution was saved and the discrete data interpolated as denoted by $T(r,\theta)$. This was the common input for the evaluation of specific thermoelastic solutions:

(i) $u_r(r,\theta)$ for either boundary condition (B1) or (B2) using the methodology of Sec. 4 with 50 retained harmonics under a state of plane stress
(ii) $u_r^{\mathrm{FE}}(r,\theta)$ for either boundary condition (B1) or (B2) using the finite element method [19] under a state of plane stress. To achieve (B2), a second composite ring was considered to be bonded to the annular component.

In producing the results from (ii), the annular component was discretized into a (r,θ) grid of dimension 7×361, large enough to produce grid independent finite element elastic solutions for the particular temperature distribution $T(r,\theta)$. A comparison of normalized results from (i) and (ii) is shown in Fig. 3. For the fixed outer boundary condition (B1), the maximum relative error is below 0.5%. For the resilient outer boundary condition (B2), the maximum relative error is just above 1%. Similar errors were predicted for the other output variables. These small differences are attributable to interpolation errors in the evaluation of the temperature harmonics and their derivatives in Eqs. (14) and (15). These errors arise from the finite element representation of $T(r,\theta)$ in this validation process, but would not be present in the general

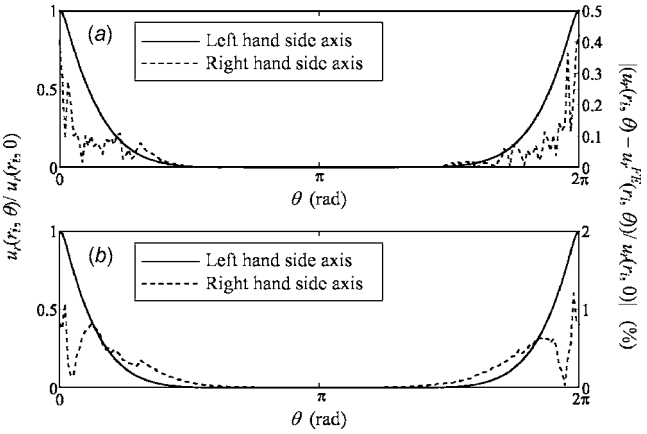

Fig. 3 Normalized solutions and relative errors between finite element and analytical solutions: (*a*) rigid outer boundary and (*b*) resilient outer boundary

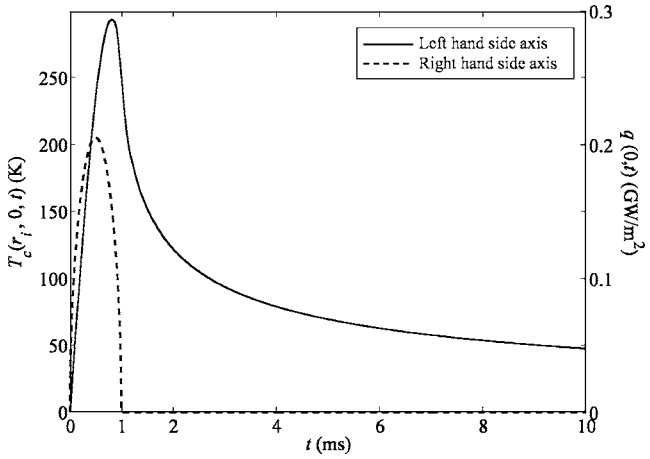

Fig. 4 Time variation of inner surface temperature at contact point $\theta=0$ together with the associated heat flux. The data in Table 1 apply.

application of the analytical method based on thermal Green's functions. It is therefore concluded that the analytical results are consistent with those produced by validated finite element software.

Further comment is also included to emphasize the fact that finer grids would be required to obtain sufficiently accurate finite element solutions corresponding to more localized temperature distributions. If the solutions are also highly transient, either a time dependent grid could be used, otherwise a conservatively fine grid with implications for long execution times.

6.2 Further Practical Results. An example of a spinning rotor making dynamic contact with an auxiliary bearing bushing is considered. Typically, an auxiliary bearing is a relatively short component so that a state of plane stress is appropriate. The thermal problem alone has been covered in Ref. [18] so an outline only of this aspect is presented. For a single contact event starting at $\theta=t=0$, the heat flux per unit length into the bearing arises from surface slip within a Hertzian contact zone. It is expressible as

$$q(\theta,t) = \begin{cases} q_0\sqrt{\phi(t)^2\theta_0^2 - \theta^2} & -\phi(t)\theta_0 \leqslant \theta \leqslant \phi(t)\theta_0 \\ 0 & \text{otherwise} \end{cases} \tag{51}$$

where $2\theta_0$ is the maximum angular extent of the contact zone. It is taken that the contact arises between the rotor and auxiliary bearing in the presence of radial clearance, hence in a nonconformal manner. The form of $\phi(t) \geqslant 0$ defines the dynamic nature of the contact event. If it involves a finite duration bounce type rotor motion, then $\phi(t)=\sin \omega_c t$ is a useful approximation when $0 \leqslant t \leqslant \pi/\omega_c$, with $\phi(t)=0$ otherwise. The outer and side faces of the auxiliary bearing are adiabatic and the initial condition is one of zero temperature.

The contact induced temperature is given by

$$T_c(r,\theta,t) = l_b \sum_{n=-\infty}^{\infty} T_{cn}(r,t)e^{in\theta} \tag{52}$$

where l_b is the bearing length and

$$T_{cn}(r,t) = \int_{\tau=0}^{t}\int_{\varphi=-\phi(\tau)\theta_0}^{\phi(\tau)\theta_0} e^{-in\varphi}q(\varphi,\tau)d\varphi T_{Gn}(r,t-\tau)d\tau$$

$$= q_0\int_{\tau=0}^{t} \frac{\pi\theta_0\phi(\tau)}{n} J_1(n\theta_0\phi(\tau))T_{Gn}(r,t-\tau)d\tau \tag{53}$$

whenever $n \neq 0$; otherwise, $T_{c0}(r,t)=q_0\int_{\tau=0}^{t}\frac{1}{2}\pi\theta_0^2\phi(\tau)^2 T_{G0}(r,t-\tau)d\tau$. The alternative form of T_G in Eq. (46) may be used to modify Eq. (53) to the form

$$T_c(r,\theta,t) = T_{cH}(r,\theta,t) - \frac{1}{2\pi K_b}\int_0^t g_b(\tau)T_{cH}(r,\theta,t-\tau)d\tau$$

$$+ \sum_{n=-\infty}^{\infty} T_{cRn}(r,t)e^{in\theta} \tag{54}$$

with a remainder series that has an improved rate of convergence. Details are given in Ref. [18].

Thermoelastic results are now evaluated for the data given in Table 1. The length/diameter ratio for the auxiliary bearing is $l_b/2r_i=0.15$, which justifies the use of a plane stress condition. The angular extent of the contact zone was determined from a contact force of 10 kN applied from a 19.5 mm radius steel rotor having a radial clearance of 0.5 mm. Figures 4 and 5 show the transient nature of the contact induced temperature, which was evaluated from Eq. (54) with the remainder series truncated at 50 harmonics. If the direct form of Eq. (52) were used, the short time scale representations would be poor. The temperature rises rapidly during the contact period and just after the contact event has finished (1 ms), the localized behavior is clear. This is followed by a transient decrease to lower and more diffuse temperatures.

The thermoelastic displacements and stresses follow directly from the convolution integrals:

$$\mathbf{w}_c(r,\theta,t) = l_b\sum_{n=-\infty}^{\infty}\mathbf{w}_{cn}(r,t)e^{in\theta} \quad \boldsymbol{\sigma}_c(r,\theta,t) = l_b\sum_{n=-\infty}^{\infty}\boldsymbol{\sigma}_{cn}(r,t)e^{in\theta} \tag{55}$$

where

$$\mathbf{w}_{cn}(r,t) = \int_{\tau=0}^{t}\int_{\varphi=-\phi(\tau)\theta_0}^{\phi(\tau)\theta_0} e^{-in\varphi}q(\varphi,\tau)d\varphi\mathbf{w}_{Gn}(r,t-\tau)d\tau$$

$$\boldsymbol{\sigma}_{cn}(r,t) = \int_{\tau=0}^{t}\int_{\varphi=-\phi(\tau)\theta_0}^{\phi(\tau)\theta_0} e^{-in\varphi}q(\varphi,\tau)d\varphi\boldsymbol{\sigma}_{Gn}(r,t-\tau)d\tau \tag{56}$$

Figure 6 shows the variation of the thermoelastic Green's function $\mathbf{w}_G$ on the inner bearing surface at a particular value of time. The radial and tangential components were evaluated using series truncated at 50 harmonics, either directly from Eq. (46) or from the modified form of Eq. (50). The truncated form of Eq. (46) does not efficiently represent the localized nature of $\mathbf{u}_G$, which is evident from the oscillatory variations on the inner surface. For this reason, the improved form of Eq. (50) was used to evaluate the contact induced thermoelastic displacement:

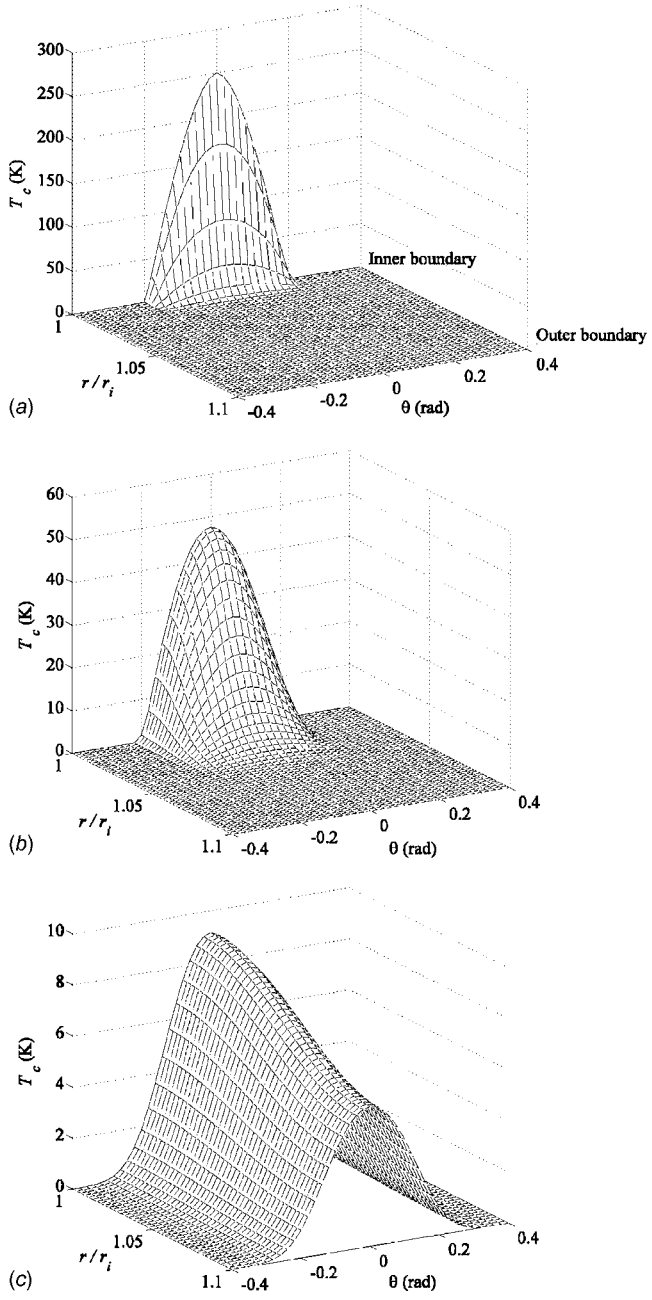

Fig. 5 Contact induced temperature distributions at (*a*) t =1 ms, (*b*) t=10 ms, and (*c*) t=100 ms

$$\mathbf{w}_c(r,\theta,t) = l_b\left[\bar{\mathbf{w}}_{cH}(r,\theta,t) + \sum_{n=-\infty}^{\infty} \mathbf{w}_{cRn}(r,t)e^{in\theta}\right] \tag{57}$$

where

$$\bar{\mathbf{w}}_{cH}(r,\theta,t) = \int_{\tau=0}^{t}\int_{\varphi=-\phi(\tau)\theta_0}^{\phi(\tau)\theta_0} q(\varphi,\tau)\bar{\mathbf{w}}_{GH}(r,\theta-\varphi,t-\tau)d\varphi d\tau$$

$$\mathbf{w}_{cRn}(r,t) = \int_{\tau=0}^{t}\int_{\varphi=-\phi(\tau)\theta_0}^{\phi(\tau)\theta_0} e^{-in\varphi}q(\varphi,\tau)d\varphi\mathbf{w}_{GRn}(r,t-\tau)d\tau \tag{58}$$

The contact induced thermoelastic displacements were evaluated for the rigid (B1) and resiliently (B2) mounted cases by using Eqs. (36) and (43), respectively. Figure 7 shows the time variation of the radial displacements on the inner and outer surfaces at θ =0. The corresponding nature of the displacement distributions is shown in Figs. 8 and 9. The transient distortion of the outer surface in the resiliently mounted case would certainly be of interest for specifications associated with the auxiliary bearing mounting arrangement. For example, a preload could be applied to prevent debonding with elastomeric mounting material. The displacement of the inner surface also has implications for loss of clearance with the rotor, particularly if the rotor dynamics cause repeated contacts to occur.

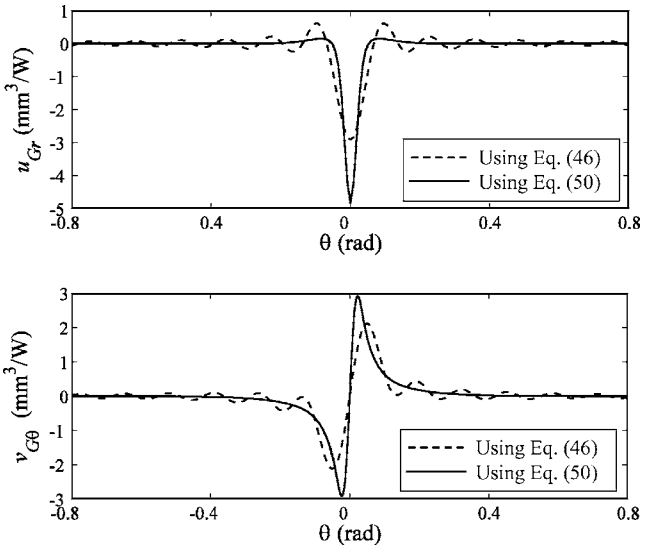

Fig. 6 Comparison of inner surface radial and tangential thermoelastic displacements of Green's function evaluated at t =10 ms. The dashed line corresponds to a truncated series of 50 harmonics from Eq. (46), while the solid line corresponds to a truncated series of 50 harmonics from Eq. (50).

The evaluation of stresses from the direct summation in Eq. (56) with 50 harmonics was limited in accuracy at short time scales by the localized nature of the problem. Therefore, the results obtained for t=1 ms are not presented. The longer time results, covering both mounting cases, are shown in Figs. 10–13. Radial tensile stresses are predicted on the outer boundary at t =10 ms, which then become compressive at the later time of t =1 s. The level of preload to prevent overall tensile stresses could be assessed from such predictions. The von Mises stresses are

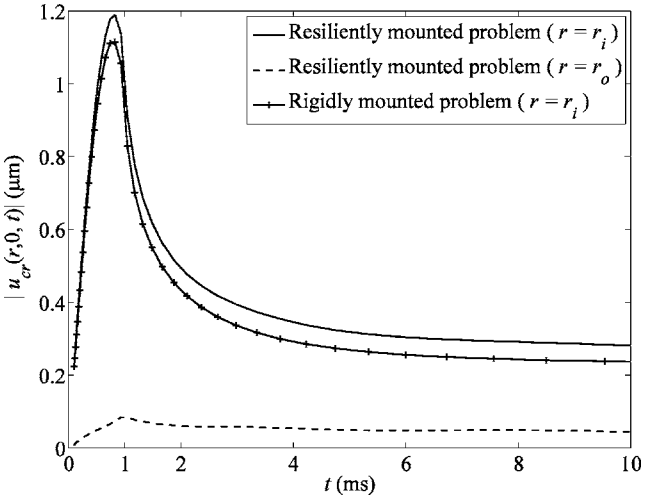

Fig. 7 Time variation of thermoelastic radial displacements at θ=0. The data in Table 1 apply.

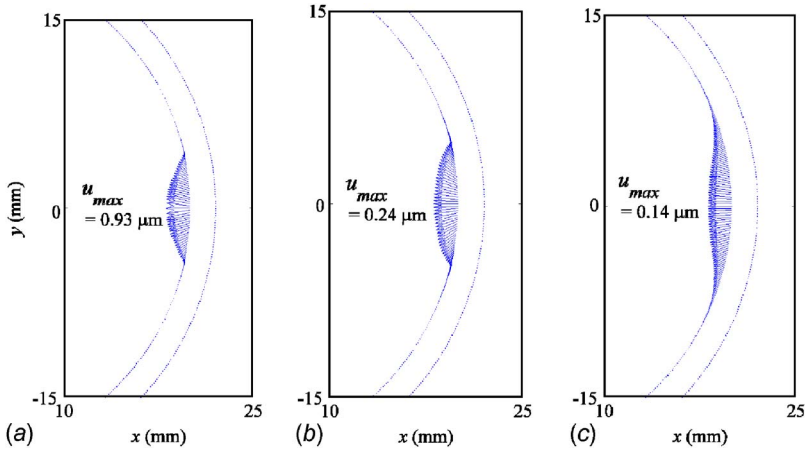

Fig. 8 Thermoelastic surface distortion of the rigidly mounted bearing at (*a*) *t*=1 ms, (*b*) *t*=10 ms, and (*c*) *t*=100 ms

below yield values at the considered time points. However, repeated contacts could result in a dynamic accumulation of stress levels. This is the subject of further work.

7 Conclusions

A study of the localized and transient thermoelastic problem for an annular component has been presented. The transient behavior prevents the application of standard potential function thermoelastic methods. A finite element approach to the problem would also involve the complexity of a time varying grid with fine spacing to encapsulate the localized parameter variations. A method was therefore developed to solve for the pseudostatic harmonic displacement components from a state space formulation. This allows for convenient implementation of different mechanical boundary conditions, as demonstrated for rigid and resiliently mounted cases. The general forms of the thermoelastic Green's functions were presented.

The application to problems involving highly localized tran-

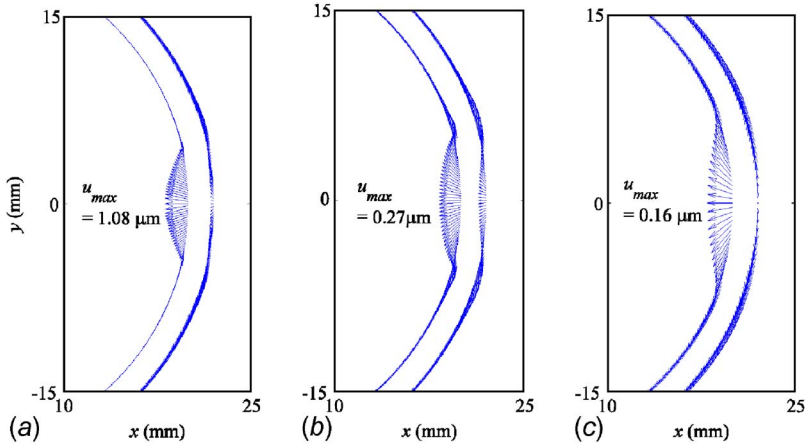

Fig. 9 Thermoelastic surface distortions of the resiliently mounted bearing at (*a*) *t*=1 ms, (*b*) *t*=10 ms, and (*c*) *t*=100 ms

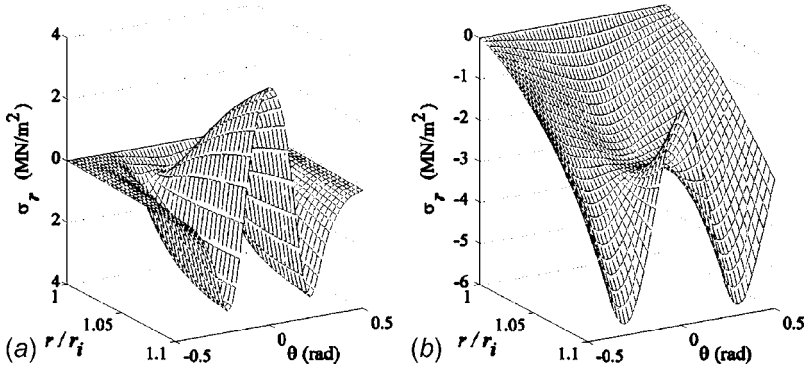

Fig. 10 Thermoelastic radial stress distributions for the rigidly mounted bearing at (*a*) *t*=10 ms and (*b*) *t*=1 s

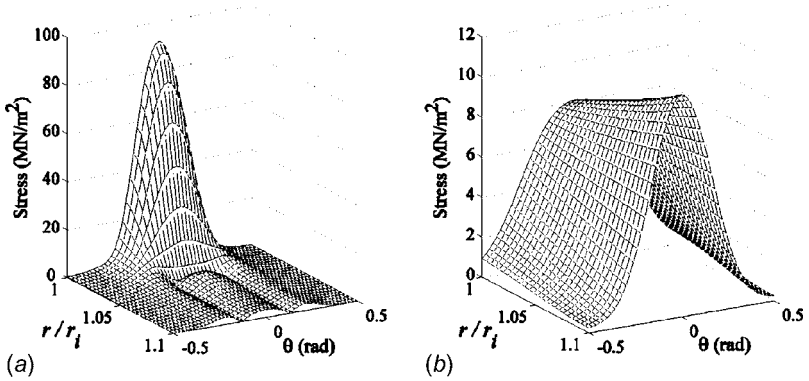

Fig. 11 Thermoelastic von Mises stress distributions for the rigidly mounted bearing at (*a*) *t*=10 ms and (*b*) *t*=1 s

sient heating, as is appropriate to contact based problems, will lead to poor rates of convergence in the direct series representations. However, the localized thermoelastic behavior may be extracted by introducing half space solutions, for which the residual Fourier series have an improved rate of convergence. The success of this method relies on the availability of Fourier components from the half space forms in order that the residual series may be formed. For the displacements, this was realizable by continuation of the half space surface displacements of Barber and Martin-Moran into the annular region. The same technique could not be applied to the half space surface stress components, which are always zero. Until half space stresses can be expanded in convenient Fourier series forms in the enveloped annular region, a localized stress solution will have a slow convergence rate at short time scales.

Results were obtained for a typical problem involving contact between a spinning rotor and an auxiliary bearing bushing. The localized deformation of the inner surface was determined successfully over a complete range of time scales. However, the thermoelastic stress solution accuracy at very short time scales was limited by the level of Fourier series truncation. Nonetheless, the method allows many useful stress predictions to be made, particularly at the outer surface boundary where tensile stresses will be important for the life prediction of auxiliary bearings.

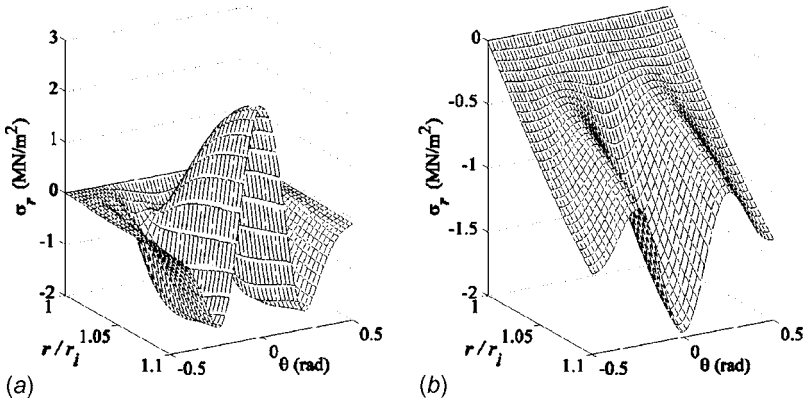

Fig. 12 Thermoelastic radial stress distributions for the resiliently mounted bearing at (*a*) *t*=10 ms and (*b*) *t*=1 s

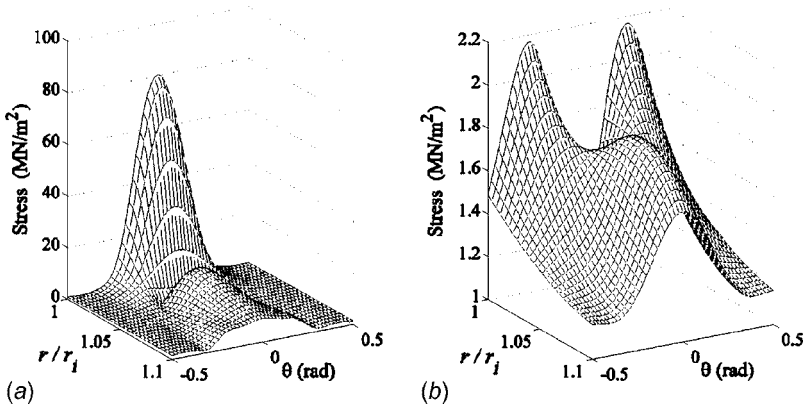

Fig. 13 Thermoelastic von Mises stress distributions for the resiliently mounted bearing at (*a*) *t*=10 ms and (*b*) *t*=1 s

Acknowledgment

The authors acknowledge the receipt of funding from an Overseas Research Student award, a Postgraduate Studentship from the University of Bath, together with support from EPSRC Platform Grant No. GR/S64448/01.

Appendix: Fourier Decomposition of Half Space Forms

Firstly, it is noted [11] that

$$\frac{e^{-\rho^2/4\kappa_b t}}{2t} = \sum_{n=-\infty}^{\infty} a_n(r,t)e^{in\theta} \tag{A1}$$

where $\rho=\sqrt{r^2+r_i^2-2rr_i\cos\theta}$ and

$$a_n(r,t) = \frac{\kappa_b}{r_i^2}\int_0^{\infty} J_n(x)J_n(xr/r_i)xe^{-\kappa_b x^2 t/r_i^2}dx \tag{A2}$$

Hence,

$$e^{-\rho^2/4\kappa_b t} = \sum_{n=-\infty}^{\infty} c_n(r,t)e^{in\theta} \tag{A3}$$

where $c_n(r,t)=2ta_n(r,t)$. It is now noted that if $R=\rho/2\sqrt{\kappa_b t}$, then

$$\frac{1-e^{-R^2}}{R^2} = \int_0^1 e^{-R^2 u}du = \sum_{n=-\infty}^{\infty} b_n(r,t)e^{in\theta} \tag{A4}$$

where, after some manipulation involving a change of integration variable, $v=1/u$, which introduces the first order exponential integral E_1,

$$b_n(r,t) = \int_0^1 c_n(r,t/u)du = \frac{2\kappa_b t}{r_i^2}\int_0^{\infty} J_n(x)J_n(xr/r_i)xE_1(\kappa_b x^2 t/r_i^2)dx \tag{A5}$$

It is also possible to express

$$F_1(R) = \frac{2}{\sqrt{\pi}}\frac{e^{-R^2}}{R}\int_0^R e^{S^2}dS = \frac{2}{\sqrt{\pi}}\int_0^1 e^{-\rho^2(1-u^2)/4\kappa_b t}du$$

$$= \sum_{n=-\infty}^{\infty} d_n(r,t)e^{in\theta} \tag{A6}$$

Again, a change of integration variable, $v=1/(1-u^2)$, yields

$$d_n(r,t) = \frac{2}{\sqrt{\pi}}\int_0^1 c_n(r,t/(1-u^2))du$$

$$= \frac{2\kappa_b t}{\sqrt{\pi}r_i^2}\int_0^{\infty} J_n(x)J_n(xr/r_i)xe^{\kappa_b x^2 t/2r_i^2}K_0(\kappa_b x^2 t/2r_i^2)dx \tag{A7}$$

It now follows from Eqs. (47) that

$$u_{GHx}(R,t) = \frac{\alpha_e}{\pi\rho_b c_b\sqrt{\kappa_b t}}\frac{(1+\nu)}{(\beta+\nu)}\sum_{n=-\infty}^{\infty} d_n(r,t)e^{in\theta}$$

$$u_{GHy}(R,t) = \frac{\alpha_e}{\pi\rho_b c_b\sqrt{\kappa_b t}}\frac{(1+\nu)}{(\beta+\nu)}\sum_{n=-\infty}^{\infty} b_n(r,t)e^{in\theta}R \tag{A8}$$

The expansion of the radial displacement term in Eq. (49) is then achieved with the coefficients

$$\bar{u}_{GHrn}(r,t) = -\frac{\alpha_e}{2\pi\rho_b c_b\sqrt{\kappa_b t}}\frac{(1+\nu)}{(\beta+\nu)}[d_{n-1}(r,t)+d_{n+1}(r,t)] \tag{A9}$$

The complication of the multiplier R in Eq. (A8) may be overcome by noting that the singularity in the Green's function only occurs on $r=r_i$, in which case $R\sim r_i\tan\theta$ as $\theta\to 0$. Therefore, the coefficients of the tangential component in Eq. (49) are given by

$$\bar{v}_{GH\theta n}(r,t) = -i\frac{\alpha_e}{4\pi\rho_b c_b\kappa_b t}\frac{(1+\nu)}{(\beta+\nu)}[b_{n-1}(r,t)-b_{n+1}(r,t)] \tag{A10}$$

References

[1] Cole, M. O. T., Keogh, P. S., and Burrows, C. R., 2002, "The Rotor Behavior of a Rolling Element Auxiliary Bearing Following Rotor Impact," ASME J. Tribol., **124**, pp. 406–413.
[2] Johnson, K. L., 1999, *Contact Mechanics*, Cambridge University Press, Cambridge.
[3] Harris, T. A., 1966, *Rolling Bearing Analysis*, Wiley, New York.
[4] Chao, C. K., and Tan, C. J., 2000, "On the General Solutions for Annular Problems With a Point Heat Source," ASME J. Appl. Mech., **67**, pp. 511–518.
[5] Sternberg, E., and McDowell, E. L., 1957, "On the Steady-State Thermoelastic Problem for the Half-Space," J. Appl. Math., **14**, pp. 381–398.
[6] Barber, J. R., and Martin-Moran, C. J., 1982, "Green's Function for Transient Thermoelastic Contact Problems for the Half-Plane," Wear, **79**, pp. 11–19.
[7] Azarkhin, A., and Barber, J. R., 1988, "Green's Functions for Subsurface Thermal Stresses Due to Surface Heating," J. Therm. Stresses, **11**, pp. 1–16.
[8] Yevtushenko, A. A., and Kovalenko, Y. V., 1995, "The Interaction of Frictional Heating and Wear at a Transient Sliding Contact," J. Appl. Math. Mech., **59**(3), 459–466.
[9] Yevtushenko, A. A., and Kulchytsky-Zhyhailo, R. D., 1995, "Axi-Symmetrical Transient Contact Problem for Sliding Bodies With Heat Generation," Int. J. Solids Struct., **32**, pp. 2369–2376.
[10] Liu, S., and Wang, Q., 2003, "Transient Thermoelastic Stress Fields in a Half-Space," ASME J. Tribol., **125**, pp. 33–43.
[11] Carslaw, H. S., and Jaeger, J. C., 1960, *Conduction of Heat in Solids*, 2nd ed., Oxford University Press, Oxford.
[12] Tarn, J. Q., and Wang, Y. M., 2001, "Laminated Composite Tubes Under Extension, Torsion, Bending, Shearing and Pressuring: A State Space Approach," Int. J. Solids Struct., **38**, pp. 9053–9075.
[13] Tarn, J. Q., 2002, "A State Space Formalism for Anisotropic Elasticity. Part II: Cylindrical Anisotropy," Int. J. Solids Struct., **39**, pp. 5157–5172.
[14] Ezzat, M. A., El-Karamany, A. S., and Samaan, A. A., 2004, "The Dependence of the Modulus of Elasticity on Reference Temperature in Generalized Thermoelasticity With Thermal Relaxation," Appl. Math. Comput., **147**, pp. 169–189.
[15] El-Maghraby, N. M., and Yossef, H. M., 2004, "State Space Approach to Generalized Thermoelastic Problem With Thermomechanical Shock," Appl. Math. Comput., **156**, pp. 577–586.
[16] Timoshenko, S. P., and Goodier, J. N., 1970, *Theory of Elasticity*, McGraw-Hill, New York.
[17] DiStefano, J. J., Williams, I. J., and Stubberud, A. J., 1990, *Outline of Theory and Problems of Feedback and Control Systems*, 2nd ed., McGraw-Hill, New York.
[18] Keogh, P. S., and Yong, W. Y., 2007, "Thermal Assessment of Dynamic Rotor/Auxiliary Bearing Contact Events," ASME J. Tribol., **129**, pp. 143–152.
[19] ANSYS Multiphysics™, © 2005 ANSYS, Inc.